Inexpensive and Non-Fluorinated Superhydrophobic Concrete Coating for Anti-Icing and Anti-Corrosion

Jinlong Song[1, 2], *Yuxiang Li*[1], *Wei Xu*[3], *Hong Liu*[4*], *Yao Lu*[5*]

1 Key Laboratory for Precision and Non-traditional Machining Technology of the Ministry of Education, Dalian University of Technology, Dalian 116024, China

2 Collaborative Innovation Center of Major Machine Manufacturing in Liaoning, Dalian University of Technology, Dalian 116024, China

3 School of Mechanics and Civil Engineering, China University of Mining and Technology (Beijing), 100083, China

4 Key Laboratory of Theoretical Chemistry of Environment Ministry of Education, School of Chemistry and Environment, South China Normal University, Guangzhou 510006, China

5 Department of Mechanical Engineering, University College London, London, WC1E 7JE, UK.

Corresponding Author

E-mail: Hong Liu (hliujlu@gmail.com); Yao Lu (yao.lu@ucl.ac.uk)

Abstract: Reinforced concrete is widely used in civil engineering due to its outstanding mechanical properties and low cost. However, icing and corrosion on concrete-based facilities such as roads, dams, and bridges often cause safety issues. Superhydrophobic surface with completely water-repellent properties that are inspired by the lotus leaf in nature, has great potential to solve this problem, however, most state-of-the-art and commercial superhydrophobic coatings are expensive and weak in mechanical robustness for large-scale application on concrete. Here, we developed an inexpensive, non-fluorinated, and robust superhydrophobic concrete (S-concrete) coating with a contact angle of 160 ± 1° and sliding angle of 6.5 ± 0.5°. This coating had a high surface mechanical strength and retained superhydrophobicity after blade scratch for several times or sandpaper abrasion for 20 m distance. The robust S-concrete coating also had a good anti-icing ability, a low deicing force, and a high corrosion resistance, which is expected to be applied on roads, buildings, bridges, and many other concrete-based facilities in large scale for anti-icing and anti-corrosion purposes.

Keywords: Superhydrophobic; Concrete coating; Mechanical strength

1 Introduction

Reinforced concrete is widely used in civil engineering due to its outstanding mechanical properties and low cost. However, concrete is inherently porous and hydrophilic that often results in surface icing from freezing water and cold water in a freezing environment. The adhered ice makes concrete road slippery and greatly increases traffic accident risk. For example, slippery roads due to ice are a major cause of road traffic accidents in Sweden during the winter.[1] The porous and hydrophilic concrete also easily results in the corrosion of the reinforcing rebar inside from corrosive environment. Corrosive ions (Cl^-, SO_4^{2-}) and acid from sea, deicing salt, and industrial wastes often corrode the reinforcing rebar.[2] The thinning of the rebar reduces the strength and carrying capacity of concrete. Moreover, the corrosion expansion of the rebar will further destroy the concrete structures, resulting in burst and flake. Concrete components in seaport projects can burst and flake due to corrosion of seawater, and the cost of repairs caused by concrete corrosion is very high. From the perspective of sustainable development, the focus of research on concrete is switching from improving its mechanical properties to improving its durability. In addition to adjusting the mix ratio and adding a variety of admixtures, the application of a water-repellent coating on the concrete surface is a more effective measure against ice and corrosion.

Superhydrophobic coating with completely water-repellent properties which is inspired by the lotus leaf has become a hot topic in recent years.[3,4] When a superhydrophobic coating is covered on the reinforced concrete, its high water-repellent properties will hinder the freezing water from staying on the concrete surface and stop the corrosive ions and acid from penetrating the porous concrete and contacting the reinforcing rebar. It will also greatly increase the life span of concrete materials and create more economic benefits for many large projects, such as bridges,

offshore engineering, and seaports. According to the main composition of materials, a superhydrophobic coating may include cyanoacrylates,[5] epoxy resin,[6] polyelectrolyte complexes,[7] ammonium polyphosphate,[8] candle soot,[4,9-11] carbon black/polybutadiene elastomeric composite,[12] wax,[13] calcium carbonate nanoparticles,[14] graphene oxide/diatomaceous earth/PDMS composite,[15] TiO_2,[3, 16] SiO_2,[17-21] PDMS,[22] Ag nanoparticles,[23] et al. However, low adhesion force between the coating and substrate, low mechanical strength, high cost, and even extensive use of fluorocarbon materials which is potentially toxic to humans indicate that the state-of-the-art methods are difficult to scale-up in large industrial concrete projects. A simultaneous demonstration of the aforementioned four features is a major challenge. In 2017, we reported a superhydrophobic concrete block by covering metal mesh and with additional fluoroalkylsilane modification in the base of the fabrication processes used for ordinary concrete block.[24] However, the use of metal mesh and fluoroalkylsilane is expensive.

In order to address the aforementioned problems, we developed an inexpensive and non-fluorinated superhydrophobic concrete coating by using low-cost cement, sand, commercial water-based stone protector, and nylon mesh which are commercially available. The resulted concrete coating had a high surface mechanical strength and still showed superhydrophobicity after blade scratch or sandpaper abrasion for 20 m distance. The superhydrophobic concrete coating also presented remarkable anti-icing and anti-corrosion properties. Since the main composition of the coating and architecture is concrete, the adhesion between the coating and substrates is very high. The superhydrophobic concrete coating can be easily applied on the outside surface of architecture, which not only protects the reinforced concrete but also would not affect the strength and carrying capacity of architecture.

2 Experiments

2.1 Fabrication of superhydrophobic concrete coating

40 g of Portland cement (PO42.5, purchased from Dalian Onoda Cement Co., Ltd.), 40 g of sand, 15 g of water, and 5 g of commercial water-based stone protector (DC-30, containing silane and siloxane, purchased from Nanxiong Dingcheng New Material Technology Co., Ltd.) were mixed and stirred for 10 minutes to form a uniform paste. The mixed paste was then brush-coated on a concrete block substrate (70 mm × 70 mm × 20 mm) with the coating thickness of ~3 mm. The outer surface of the concrete coating was covered with nylon mesh with pore size of 300 μm. Here, the mesh was used as a mold to roughen and pattern the surface. After the concrete coating was solidified, the nylon mesh was removed and a superhydrophobic concrete coating (S-concrete coating) was obtained. The ordinary concrete coating (O-concrete coating) was fabricated using the same procedure but without application of water-based stone protector and nylon mesh. The fabrication processes are shown in Fig. 1.

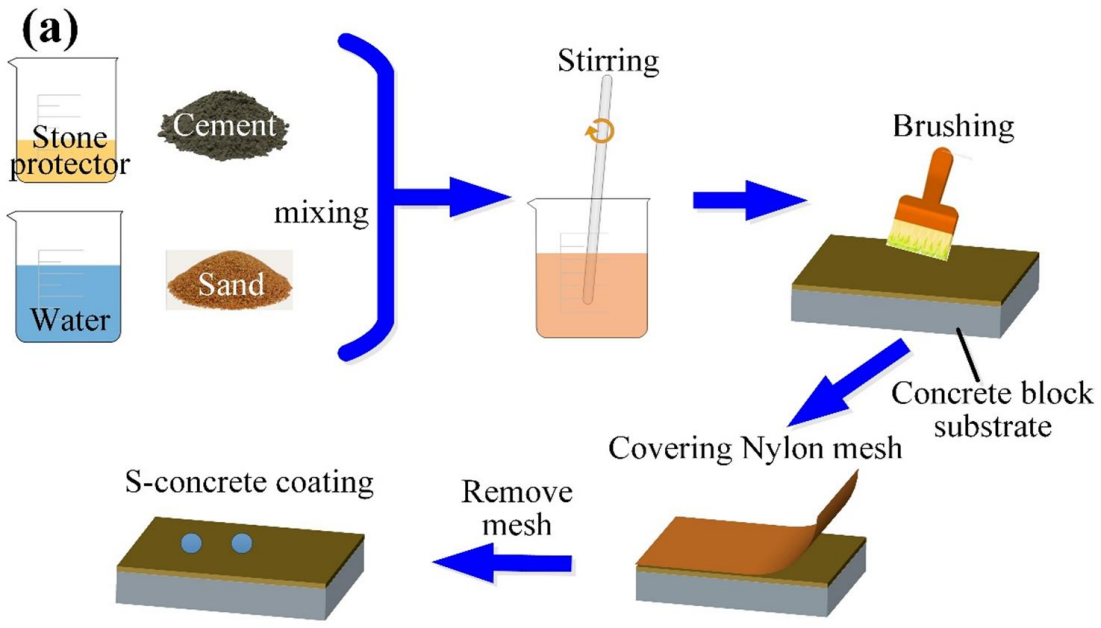

Figure 1. The schematics of the fabrication processes of the S-concrete coating.

2.2 Characterization

The contact angles and sliding angles of water droplets on the samples were measured using optical contact angle meter (Krüss, DSA100, Germany) at room temperature. The volume of water droplet was 7 μL. The surface micro-morphologies of the samples were observed using a scanning electron microscope (SEM, JSM-6360LV, Japan) at an accelerating voltage of 5 kV. The crystal structures were characterized using an X-ray diffractometer (XRD, Empyrean, Holland) with CuKα radiation (k = 0.15418 nm) at 10°-90° range and scanning step size of 2θ = 0.03939°. The elemental composition and chemical groups of the sample surfaces were examined using Fourier transform infrared spectrometer (FTIR, iN10, USA).

2.3 Surface mechanical strength test

Sandpaper abrasion and blade scratch tests were used to show the mechanical strength of the S-concrete coating. In the sandpaper abrasion test, the S-concrete coating on a circular concrete block with diameter of 60 mm was placed face-down to the 800 grit sandpaper. A 500 g weight was placed on the sample as a constant pressure. The sample was guided to move on sandpaper at a constant speed and the contact angle and sliding angle were measured every 1 m abrasion distance. In the blade scratch test, a utility blade was used to scrape the S-concrete coating with movement perpendicular to the blade edge, and the superhydrophobic effect was tested when there was noticeable powder shedding.

2.4 Anti-icing test

Two concrete blocks coated separately with the S-concrete coating and O-concrete coating were placed in an environmental chamber at an environment temperature of -10 °C. The samples had a size of 60 mm × 100 mm × 20 mm and the tilting angle was 25°. The simulated rain with a

temperature of 1 °C was applied from a 100 mL water container with 4 nozzles. The volume of rain droplet was 15 μL, and the rate of the rainfall was at 2 mL/min.

2.5 Deicing test

Two boxes without lid and bottom and with the size of 15 mm × 15 mm × 15 mm were placed separately on the S-concrete coating and O-concrete coating. Then, the concrete samples with boxes filled with water were placed horizontally in an environmental chamber at an environment temperature of -10 °C. After 4 h freezing, ice cubes with a size of 15 mm × 15 mm × 15 mm were formed and the boxes were removed. Then, the deicing force was measured using a force gauge (HP-100, Handpi Co.).

2.6 Anti-corrosion test

Two cylindrical reinforced concrete blocks with diameter of 20 mm were fabricated. Then, the S-concrete coating and O-concrete coating were separately coated on two cylindrical reinforced concrete blocks with the coating thickness of ~3 mm. All the samples were soaked in 3.5 wt% aqueous NaCl solutions at room temperature for 24 h and then tested the anti-corrosion ability. The samples were electrochemically corroded under a voltage of 26 V for 20 min in sea water (taken from the Yellow Sea, Dalian Xinghai Sea Area). After the electrochemical corrosion, the cylindrical reinforced concrete blocks were broken to observe the macro-morphology of the rebar inside. The polarization curves were obtained using a computer-controlled potentiostat (Princeton Applied Research, VersaSTAT, USA) under open circuit conditions, the sweep rate was 0.5 mV/s, and the electrochemical impedance spectroscopy (EIS) measurements were conducted in the 100 mHz to 2 MHz frequency range using a 10 mV amplitude perturbation.

3 Results and discussion

3.1 Surface morphology and wettability

Figures 2(a) and 2(b) show the macro and micro morphology of the S-concrete coating and O-concrete coating. The outside surface of the O-concrete coating was very smooth, while the outside surface of the S-concrete coating was covered with square-like convex structures with the size of 300 μm which was replicated from nylon mesh, as shown in Fig. S1. From the magnified view, both the O-concrete coating and the S-concrete coating were very rough and composed of micro/nanometer-scale particles. From the XRD patterns shown in Fig. 2(c), we learnt that the main composition of the O-concrete coating and S-concrete coating were similar, both composed of silica, calcium hydroxide, ettringite, and calcium silicate hydrate. Although the main compositions of the micro/nanometer-scale particles from the O-concrete coating and S-concrete coating are similar from XRD patterns, the C-H groups which can effectively reduce the surface energy, were only detected on the S-concrete coating. It is well known that constructing surface microstructures and lowering the surface energy at the same time is an effective way to obtain superhydrophobicity. We wondered if the O-concrete coating with micro/nanometer-scale particles can obtain superhydrophobicity after modification with water-based stone protector. Then, we modified the O-concrete coating by dipping and brushing 5 wt% aqueous solution of water-based stone protector. However, the experimental results show that the O-concrete coating after modification with water-based stone protector only shows hydrophobicity with contact angles of 90-100°, as shown in Fig. S2. Thus, the coexistence of square-like convex structures, micro/nanometer-scale particles, and low surface energy C-H groups render the S-concrete coating superhydrophobicity. Compared with the superhydrophilicity with water contact angle of ~0° on the O-concrete coating, the water droplets

on the S-concrete coating showed globular shapes with a contact angle of 160 ± 1°, and a sliding angle of 6.5 ± 0.5°. We also studied the influence of the content of water-based stone protector in the fabrication processes of the S-concrete coating on wettability. As shown in Fig. S3, the contact angles increased initially but then slightly decreased with the increase of the content, while the sliding angle decreased firstly and increased with the increase of the content. The best superhydrophobicity was obtained when the content of water-based stone protector was 5 wt% in the concrete paste. We also studied the influence of the pore size of nylon mesh in the fabrication processes of the S-concrete coating on wettability. As shown in Fig. S4, the superhydrophobicity (water contact angle ≥ 150°) was observed on the concrete-coating for the nylon mesh with pore sizes from 37 μm to 700 μm. When the pore size was too small (e.g. 20 μm) or too large (e.g. 1150 μm, and 1500 μm), only hydrophobicity was obtained.

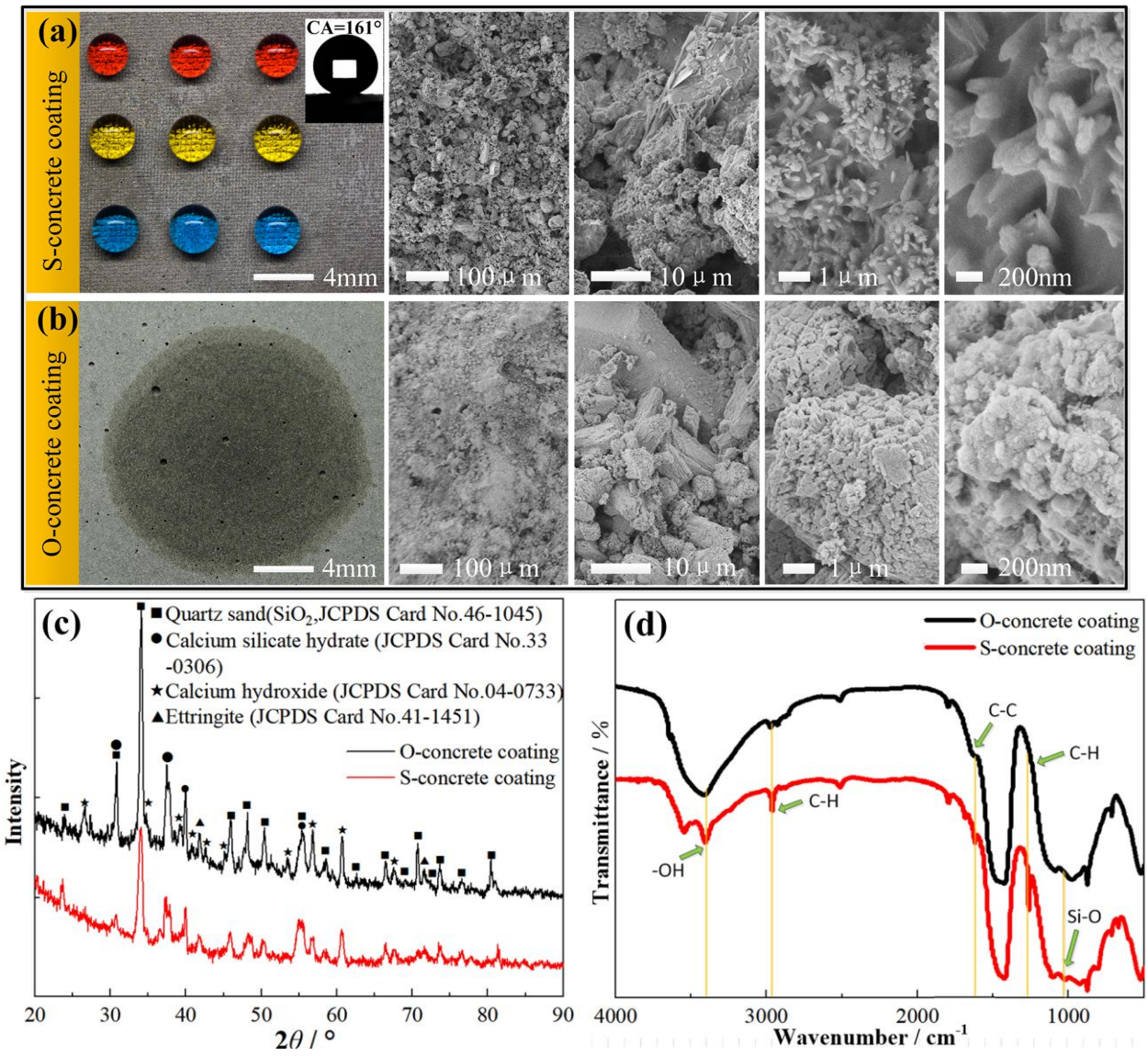

Figure 2. Surface morphology, chemical composition and wettability of the S-concrete coating and O-concrete coating: (a) the morphology and wettability of the S-concrete coating; (b) the morphology and wettability of the O-concrete coating; (c) XRD patterns of the S-concrete coating and the O-concrete coating; (d) FTIR spectra of the S-concrete coating and the O-concrete coating.

3.2 Surface mechanical strength

A scratch-resistant test was performed to demonstrate the surface mechanical strength. Blades were used to scrape the S-concrete coating with the movement perpendicular to the blade edge, followed by water dropping on the scratched area. The area that was scratched by the blade still had good superhydrophobicity, as shown in Fig. 3 (a) and **Video S1**. Fig. 3(b) and **Video S2** show the sandpaper abrasion processes of the S-concrete coating. After several meters' abrasion, water droplets on the S-concrete coating still rolled off easily without any residue. Then we carefully studied the influence of the abrasion distance on wettability. The S-concrete coating retained superhydrophobicity with a contact angle of 152° and a sliding angle of 7° even after sandpaper abrasion for 20 m. Blade scratch and sandpaper abrasion tests indicate that the developed S-concrete coating has good mechanical strength. We believe the high mechanical strength is originated from the tremendous hardness of the concrete material.

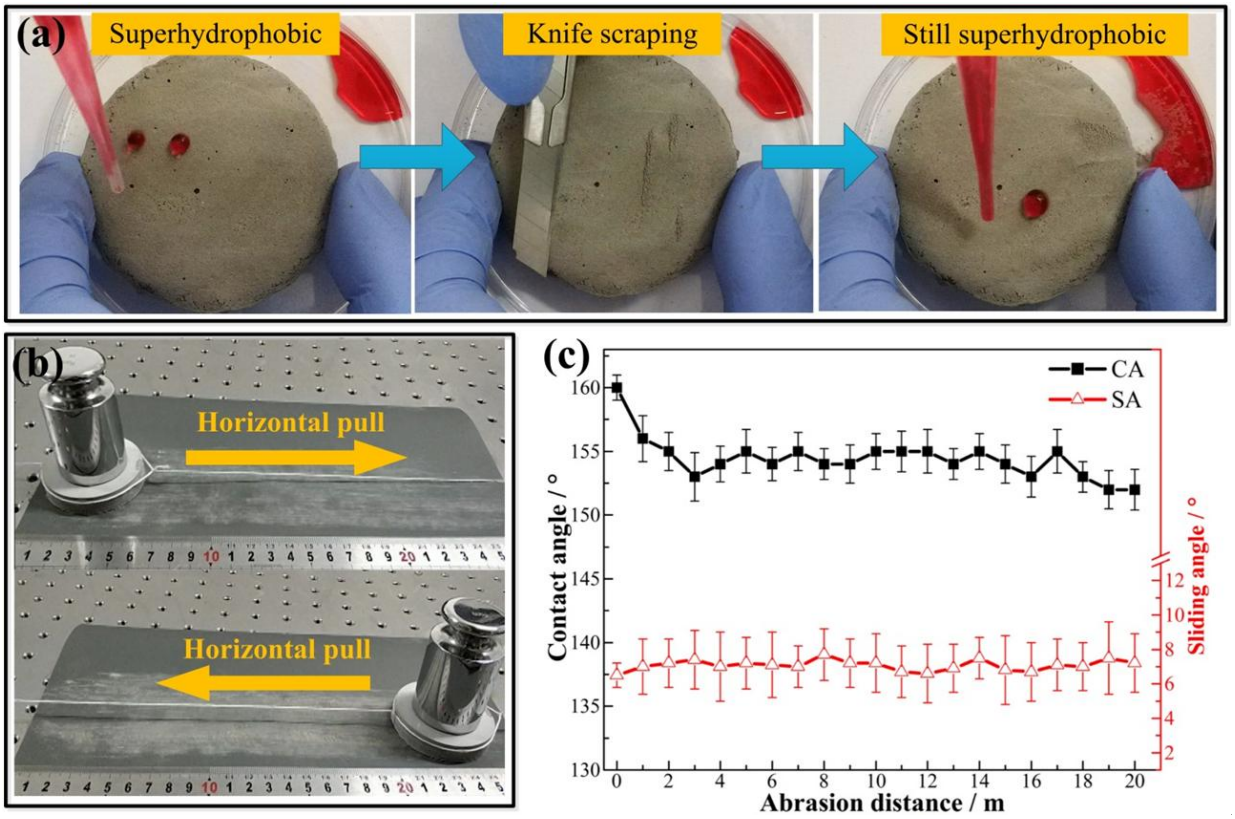

Figure 3. Surface mechanical strength tests: (a) the blade scratch processes of the S-concrete coating; (b) the sandpaper abrasion processes of the S-concrete coating; (c) the influence of abrasion distance on wettability of the S-concrete coating.

3.3 Anti-icing and deicing

Two concrete blocks coated separately with the S-concrete coating and O-concrete coating were placed in an environmental chamber with a sloping angle of 25°. Fig. 4(a) shows the schematic of the anti-icing experiment. Fig. 4(b) and **Video S3** show the anti-icing and icing processes on the S-concrete coating and O-concrete coating. The rain droplets with a temperature of 1 °C easily wetted the O-concrete coating and froze into ice under the environmental temperature of -10 °C. As the raining process continues, the ice on the O-concrete coating became thicker and thicker. However, the situation for the S-concrete coating was different. The rain droplets on the S-concrete coating rolled off completely and no ice was formed. The aforementioned results indicate the S-concrete coating has a good anti-icing ability from freezing water or cold water in a freezing environment. It's important to note that the anti-icing ability of the S-concrete coating only exists when its sloping angle larger than the sliding angle of rain droplets. When the concrete blocks were placed horizontally in the environmental chamber. Rain droplets were stayed both on the S-concrete coating and O-concrete coating and formed into ice. We then measured the deicing force in that situation and the schematic of the deicing experiment is shown in Fig. 4(c). The deicing processes on the S-concrete coating and O-concrete coating are shown in Fig. 4(d) and **Video S4**. The ice cube on the S-concrete coating was completely removed without any residue with a deicing force of 25 N, while the one on the O-concrete coating was broken with the ice residue and a deicing force of 354 N, as shown in Fig. 4(e). Low

deicing force and no ice residue on the S-concrete coating in the deicing processes would effectively reduce the deicing difficulty of horizontal roads.

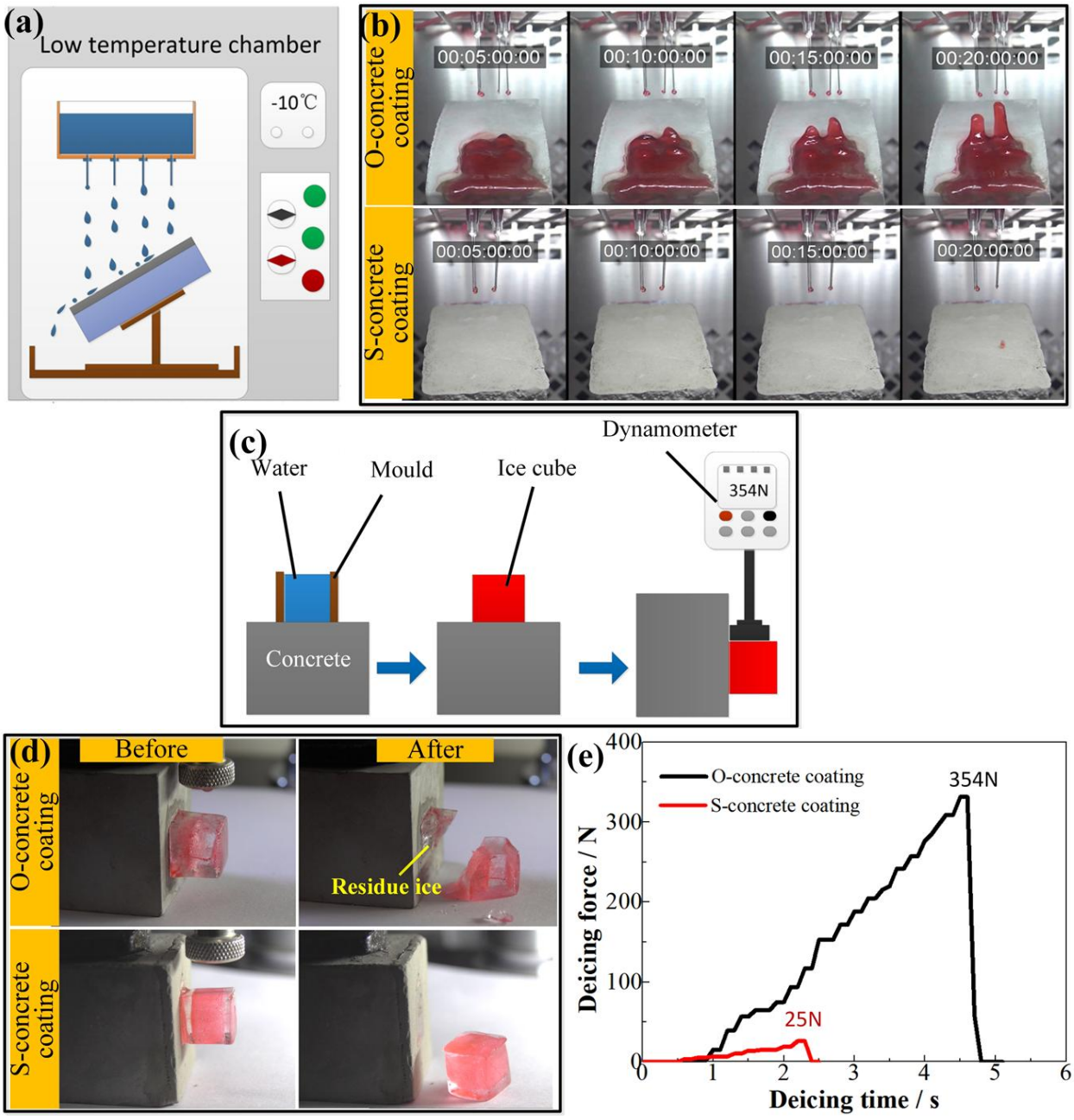

Figure 4. Anti-icing and deicing tests: (a) schematic of the anti-icing experiment; (b) the anti-icing and icing processes on the S-concrete coating and O-concrete coating; (c) schematic of the

deicing experiment; (d) the deicing processes on the S-concrete coating and O-concrete coating; (e) the deicing force for the ice cube with the ice-concrete contact area of 2.25 cm^2.

3.4 Anti-corrosion

The reinforcing rebar in the concrete plays an important role as the bone support, however, in many cases, the reinforcing rebar suffers from corrosion due to the penetration of corrosive ions into the concrete. The S-concrete coating prevents water from wetting the concrete, which in turn can block harmful components from the outside and thus protect the rebar from corrosion. Fig. 5(a) shows the schematic of the anti-corrosion test. Two reinforced concrete blocks coated separately with the S-concrete coating of 3 mm thickness and the O-concrete coating of 3 mm thickness were soaked in 3.5 wt% aqueous NaCl solutions at room temperature for 24 h first and then electrochemically corroded under a voltage of 26 V for 20 min in sea water. The electrochemical corrosion processes are shown in Fig. 5(b) and **Video S5**. We can see that with the increase of the electrochemical corrosion time, the electrolyte for the O-concrete coating became more and more turbid, indicating that the reinforcing rebar was continuously corroded. However, the electrolyte for the S-concrete coating always kept clear and translucent in the whole electrochemical corrosion processes. We then broke that two reinforced concrete blocks after electrochemical corrosion and found that the rebar inside the concrete block coated with the O-concrete coating was severely corroded and full of rust, while the rebar inside the concrete block coated with the S-concrete coating was still clean (Fig. 5(c)). Then we studied the electrochemical impedance spectra and potentiodynamic polarization curves of the rebar in the reinforced concrete blocks coated separately with the S-concrete coating and O-concrete coating in the 3.5 wt% aqueous NaCl solutions, as shown in Figs. 5(d) and 5(e). The impedance for the S-concrete coating was ten times of that for the O-concrete coating. The corrosion potential for

the S-concrete coating was 0.12 V higher than that for the O-concrete coating. The corrosion current density for the S-concrete coating was two orders magnitude lower than that for the O-concrete coating. The lower corrosion current density and higher corrosion potential and impedance are the important reasons to explain why the S-concrete coating can protect the inside rebar.

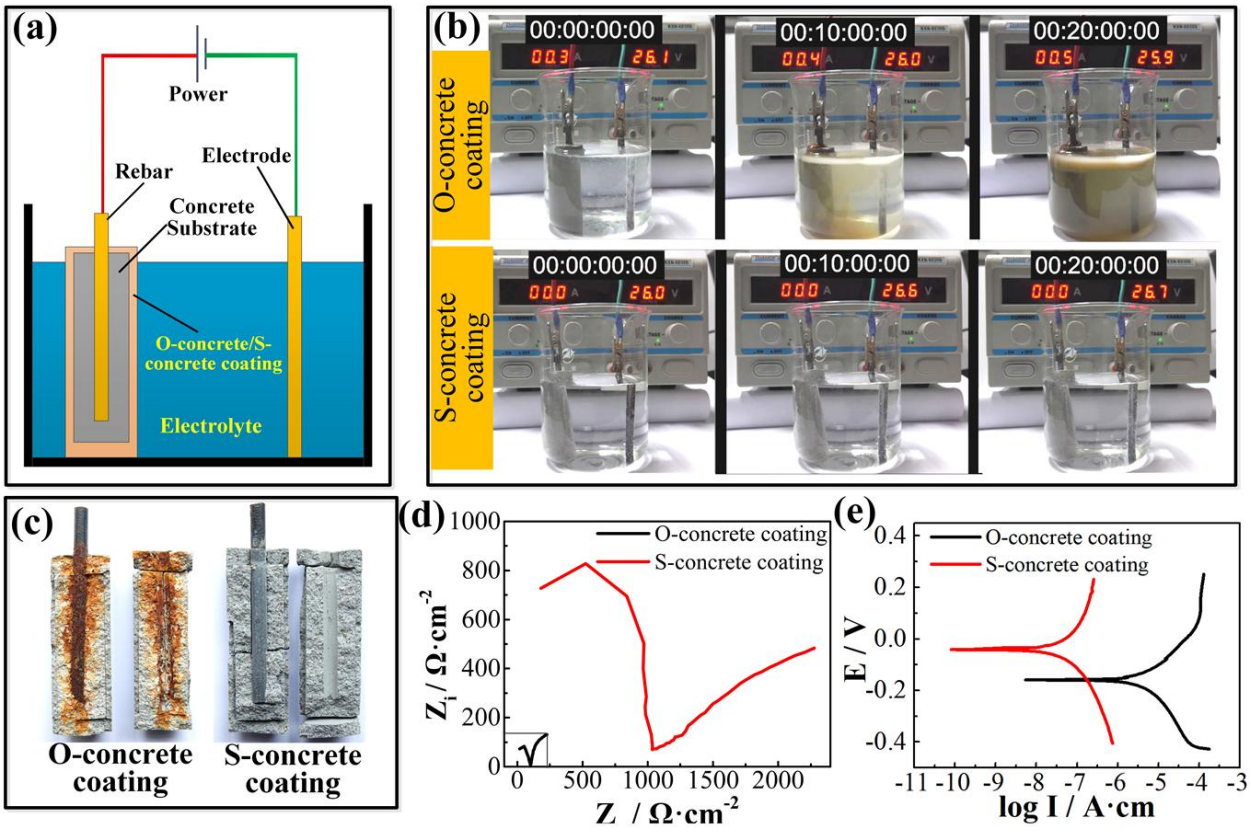

Figure 5. Anti-corrosion test: (a) schematic of the anti-corrosion test; (b) electrochemical corrosion processes under a voltage of 26 V for 20 min in sea water; (c) macro-morphology of the rebar after electrochemical corrosion; (d) the electrochemical impedance spectra of the rebar in the reinforced concrete blocks coated separately with the S-concrete coating and O-concrete coating in the 3.5 wt% aqueous NaCl solutions; (e) the potentiodynamic polarization curves of

the rebar in the reinforced concrete blocks coated separately with the S-concrete coating and O-concrete coating in the 3.5 wt% aqueous NaCl solutions.

4. Conclusions

In summary, an inexpensive and non-fluorinated superhydrophobic concrete coating (S-concrete coating) with a water contact angle of 160 ± 1° and a sliding angle of 6.5 ± 0.5° was developed using simple processes and low-cost and abundant raw materials including cement, sand, commercial water-based stone protector and nylon mesh. The superhydrophobicity was attributed to the coexistence of square-like convex structures, micro/nanometer-scale particles, and low surface energy groups. Due to the high hardness of concrete materials, the S-concrete coating with a thickness of 3 mm had a high surface mechanical strength and retained superhydrophobicity after blade scratch for several times or sandpaper abrasion for 20 m distance. The S-concrete coating also showed a good anti-icing ability for concrete substrate with the sloping angle larger than the sliding angle from freezing water or cold water in a freezing environment, and also showed a low de-icing force for horizontal concrete substrate. The water-repellent property of the S-concrete coating further made it possible to protect the rebar in the reinforcing concrete from corrosion. The S-concrete coating can be easily applied on the outside surface of architecture, which not only protects the reinforced concrete but also would not affect the strength and carrying capacity of architecture. Therefore, this economic and environmental-friendly coating is expected to be applied on buildings, bridges and many other concrete-based projects in large scale for anti-icing and anti-corrosion purposes.

Acknowledgements

This project is financially supported by National Natural Science Foundation of China (NSFC, 51605078, 21774051), the Science Fund for Creative Research Groups of NSFC (51621064),

Young Elite Scientists Sponsorship Program by CAST (YESS, 2017QNRC001), Aviation Science Fund (2017ZE63012). Y.L. acknowledges the support from EPSRC project EP/N024915/1.

References

(1) Andersson, A.; Chapman, L. The use of a temporal analogue to predict future traffic accidents and winter road conditions in Sweden. Meteorological Appl. 18 (2011) 125-136. doi：10.1002/met.186

(2) Zhang, P.; Cong, Y.; Vogel, M.; Liu, Z.; Müller, H. S.; Zhu, Y.; Zhao, T. Steel reinforcement corrosion in concrete under combined actions: The role of freeze-thaw cycles, chloride ingress, and surface impregnation. Constr. Build. Mater. 148 (2017) 113-121. doi：10.1016/j.conbuildmat.2017.05.078

(3) Lu, Y.; Sathasivam, S.; Song, J.; Crick, C.; Claire J.; Ivan, P. Robust self-cleaning surfaces that function when exposed to either air or oil. Science 347 (2015) 1132-1135. doi：10.1126/science.aaa0946

(4) Deng, X.; Mammen, L.; Butt, H.; Vollmer, D. Candle soot as a template for a transparent robust superamphiphobic coating. Science 335 (2012) 67-70. doi:10.1126/science.1207115

(5) Pan, S.; Guo, R.; Björnmalm, M.; Richardson, J. J.; Li, L.; Peng, C.; Bertleff-Zieschang, N.; Xu, W.; Jiang, J.; Caruso, F. Coatings super-repellent to ultralow surface tension liquids. Nature Mater. 17 (2018) 1040-1047. doi:10.1038/s41563-018-0178-2

(6) Peng, C.; Chen, Z.; Tiwari, M. K. All-organic superhydrophobic coatings with mechanochemical robustness and liquid impalement resistance. Nature Mater. 17 (2018) 355-360. doi:10.1038/s41563-018-0044-2

(7) Coclite, A. M.; Shi, Y.; Gleason, K. K. Grafted crystalline poly-perfluoroacrylate structures for superhydrophobic and oleophobic functional coatings. Adv. Mater. 24 (2012) 4534-4539. doi:10.1002/adma.201200682

(8) Chen, S.; Li, X.; Li, Y.; Sun, J. Intumescent flame-retardant and self-healing superhydrophobic coatings on cotton fabric. ACS Nano 9 (2015) 4070-4076. doi:10.1021/acsnano.5b00121

(9) Seo, K.; Kim, M.; Kim, D. H. Candle-based process for creating a stable superhydrophobic surface. Carbon 68 (2014) 583-596. doi:10.1016/j.carbon.2013.11.038

(10) Iqbal, R.; Majhy, B.; Sen, A. K. Facile fabrication and characterization of a PDMS-derived candle soot coated stable biocompatible superhydrophobic and superhemophobic surface. ACS Appl. Mater. Inter. 9 (2017) 31170–31180. doi:10.1021/acsami.7b09708

(11) Li, J.; Zhao, Z.; Li, D.; Tian, H.; Zha, F.; Feng, H.; Guo, L. Smart candle soot coated membranes for on-demand immiscible oil/water mixture and emulsion switchable separation. Nanoscale 9 (2017) 13610. doi:10.1039/C7NR04448H

(12) Hu, X.; Tang, C.; He, Z.; Shao, H.; Xu, K.; Mei, J.; Lau, W. M. Highly stretchable superhydrophobic composite coating based on self-adaptive deformation of hierarchical structures. Small 13 (2017) 1602353. doi:10.1002/smll.201602353

(13) Wei, W.; Lockwood, K.; Boyd, L. M.; Davidson, M. D.; Movafaghi, S.; Vahabi, H.; Khetani, S. R.; Kota, A. K. Superhydrophobic coatings with edible materials. ACS Appl. Mater. Inter. 8 (2016) 18664-18668. doi:10.1021/acsami.6b06958

(14) Chen, B.; Qiu, J.; Sakai, E.; Kanazawa, N.; Liang, R.; Feng, H. Robust and superhydrophobic surface modification by a "paint + adhesive" method: applications in self-cleaning after oil contamination and oil–water separation. ACS Appl. Mater. Inter. 8 (2016) 17659-17667. doi:10.1021/acsami.6b04108

(15) Nine, M. J.; Cole, M. A.; Johnson, L.; Tran, D. N. H.; Losic, D. Robust superhydrophobic graphene-based composite coatings with self-cleaning and corrosion barrier properties. ACS Appl. Mater. Inter. 7 (2015) 28482-28493. doi:10.1021/acsami.5b09611

(16) Ghosh, A.; Ganguly, R.; Schutzius, T. M.; Megaridis, C. M. Wettability patterning for high-rate, pumpless fluid transport on open, non-planar microfluidic platforms. Lab on A Chip 14 (2014) 1538-1550. doi:10.1039/c3lc51406d

(17) De, F. R.; Hoyos, M.; García, N.; Tiemblo, P. Superhydrophobic and highly luminescent Polyfluorene/Silica hybrid coatings deposited onto glass and cellulose-based substrates. Langmuir 31 (2015) 3718-26. doi:10.1021/acs.langmuir.5b00293

(18) Zhi, D.; Lu, Y.; Sathasivam, S.; Parkin, I. P.; Zhang, X. Large-scale fabrication of translucent and repairable superhydrophobic spray coatings with remarkable mechanical, chemical durability and UV resistance. J. Mater. Chem. A 5 (2017) 10622-10631. doi:10.1039/C7TA02488F

(19) Yang, H.; Liang, F.; Chen, Y.; Wang, Q.; Qu, X.; Yang, Z. Lotus leaf inspired robust superhydrophobic coating from strawberry-like Janus particles. NPG Asia Mater. 7 (2015) e176. doi:10.1038/am.2015.33

(20) Xu, L.; Zhu, D.; Lu, X.; Lu, Q. Transparent, thermally and mechanically stable superhydrophobic coating prepared by an electrochemical template strategy. J. Mater.Chem. A 3 (2015) 3801-3807. doi:10.1039/C4TA06944G

(21) Tuvshindorj, U.; Yildirim, A.; Ozturk, F. E.; Bayindir, M. Robust Cassie state of wetting in transparent superhydrophobic coatings. ACS Appl. Mater. Inter. 6 (2014) 9680-9688. doi:10.1021/am502117a

(22) Liu, H.; Huang, J.; Chen, Z.; Chen, G.; Zhang, K.; Al-Deyab, S. S.; Lai, Y. Robust translucent superhydrophobic PDMS/PMMA film by facile one-step spray for self-cleaning and efficient emulsion separation. Chem.Eng. J. 330 (2017) 26-35. doi:10.1016/j.cej.2017.07.114

(23) Liu, F.; Sun, F.; Pan, Q. Highly compressible and stretchable superhydrophobic coating inspired by bio-adhesion of marine mussels. J. Mater. Chem. A 2 (2014) 11365-11371. doi:10.1039/c4ta01552e

(24) Song, J.; Zhao, D.; Han, Z.; Xu, W.; Lu, Y.; Liu, X.; Liu, B.; Carmalt, C. J.; Deng, X.; Parkin, I. P. Super-robust superhydrophobic concrete. J. Mater. Chem. A 5 (2017) 14542-14550. doi:10.1039/C7TA03526H

Inexpensive and Non-Fluorinated Superhydrophobic Concrete Coating for Anti-Icing and Anti-Corrosion

Jinlong Song[1, 2], *Yuxiang Li*[1], *Wei Xu*[3], *Hong Liu*[4*], *Yao Lu*[5*]

1 Key Laboratory for Precision and Non-traditional Machining Technology of the Ministry of Education, Dalian University of Technology, Dalian 116024, China

2 Collaborative Innovation Center of Major Machine Manufacturing in Liaoning, Dalian University of Technology, Dalian 116024, China

3 School of Mechanics and Civil Engineering, China University of Mining and Technology (Beijing), 100083, China

4 Key Laboratory of Theoretical Chemistry of Environment Ministry of Education, School of Chemistry and Environment, South China Normal University, Guangzhou 510006, China

5 Department of Mechanical Engineering, University College London, London, WC1E 7JE, UK.

Corresponding Author

E-mail: Hong Liu (hliujlu@gmail.com); Yao Lu (yao.lu@ucl.ac.uk)

Abstract: Reinforced concrete is widely used in civil engineering due to its outstanding mechanical properties and low cost. However, icing and corrosion on concrete-based facilities such as roads, dams, and bridges often cause safety issues. Superhydrophobic surface with completely water-repellent properties that are inspired by the lotus leaf in nature, has great potential to solve this problem, however, most state-of-the-art and commercial superhydrophobic coatings are expensive and weak in mechanical robustness for large-scale application on concrete. Here, we developed an inexpensive, non-fluorinated, and robust superhydrophobic concrete (S-concrete) coating with a contact angle of 160 ± 1° and sliding angle of 6.5 ± 0.5°. This coating had a high surface mechanical strength and retained superhydrophobicity after blade scratch for several times or sandpaper abrasion for 20 m distance. The robust S-concrete coating also had a good anti-icing ability, a low deicing force, and a high corrosion resistance, which is expected to be applied on roads, buildings, bridges, and many other concrete-based facilities in large scale for anti-icing and anti-corrosion purposes.

Keywords: Superhydrophobic; Concrete coating; Mechanical strength

1 Introduction

Reinforced concrete is widely used in civil engineering due to its outstanding mechanical properties and low cost. However, concrete is inherently porous and hydrophilic that often results in surface icing from freezing water and cold water in a freezing environment. The adhered ice makes concrete road slippery and greatly increases traffic accident risk. For example, slippery roads due to ice are a major cause of road traffic accidents in Sweden during the winter.[1] The porous and hydrophilic concrete also easily results in the corrosion of the reinforcing rebar inside from corrosive environment. Corrosive ions (Cl^-, SO_4^{2-}) and acid from sea, deicing salt, and industrial wastes often corrode the reinforcing rebar.[2] The thinning of the rebar reduces the strength and carrying capacity of concrete. Moreover, the corrosion expansion of the rebar will further destroy the concrete structures, resulting in burst and flake. Concrete components in seaport projects can burst and flake due to corrosion of seawater, and the cost of repairs caused by concrete corrosion is very high. From the perspective of sustainable development, the focus of research on concrete is switching from improving its mechanical properties to improving its durability. In addition to adjusting the mix ratio and adding a variety of admixtures, the application of a water-repellent coating on the concrete surface is a more effective measure against ice and corrosion.

Superhydrophobic coating with completely water-repellent properties which is inspired by the lotus leaf has become a hot topic in recent years.[3,4] When a superhydrophobic coating is covered on the reinforced concrete, its high water-repellent properties will hinder the freezing water from staying on the concrete surface and stop the corrosive ions and acid from penetrating the porous concrete and contacting the reinforcing rebar. It will also greatly increase the life span of concrete materials and create more economic benefits for many large projects, such as bridges,

offshore engineering, and seaports. According to the main composition of materials, a superhydrophobic coating may include cyanoacrylates,[5] epoxy resin,[6] polyelectrolyte complexes,[7] ammonium polyphosphate,[8] candle soot,[4,9-11] carbon black/polybutadiene elastomeric composite,[12] wax,[13] calcium carbonate nanoparticles,[14] graphene oxide/diatomaceous earth/PDMS composite,[15] TiO_2,[3, 16] SiO_2,[17-21] PDMS,[22] Ag nanoparticles,[23] et al. However, low adhesion force between the coating and substrate, low mechanical strength, high cost, and even extensive use of fluorocarbon materials which is potentially toxic to humans indicate that the state-of-the-art methods are difficult to scale-up in large industrial concrete projects. A simultaneous demonstration of the aforementioned four features is a major challenge. In 2017, we reported a superhydrophobic concrete block by covering metal mesh and with additional fluoroalkylsilane modification in the base of the fabrication processes used for ordinary concrete block.[24] However, the use of metal mesh and fluoroalkylsilane is expensive.

In order to address the aforementioned problems, we developed an inexpensive and non-fluorinated superhydrophobic concrete coating by using low-cost cement, sand, commercial water-based stone protector, and nylon mesh which are commercially available. The resulted concrete coating had a high surface mechanical strength and still showed superhydrophobicity after blade scratch or sandpaper abrasion for 20 m distance. The superhydrophobic concrete coating also presented remarkable anti-icing and anti-corrosion properties. Since the main composition of the coating and architecture is concrete, the adhesion between the coating and substrates is very high. The superhydrophobic concrete coating can be easily applied on the outside surface of architecture, which not only protects the reinforced concrete but also would not affect the strength and carrying capacity of architecture.

2 Experiments

2.1 Fabrication of superhydrophobic concrete coating

40 g of Portland cement (PO42.5, purchased from Dalian Onoda Cement Co., Ltd.), 40 g of sand, 15 g of water, and 5 g of commercial water-based stone protector (DC-30, containing silane and siloxane, purchased from Nanxiong Dingcheng New Material Technology Co., Ltd.) were mixed and stirred for 10 minutes to form a uniform paste. The mixed paste was then brush-coated on a concrete block substrate (70 mm × 70 mm × 20 mm) with the coating thickness of ~3 mm. The outer surface of the concrete coating was covered with nylon mesh with pore size of 300 μm. Here, the mesh was used as a mold to roughen and pattern the surface. After the concrete coating was solidified, the nylon mesh was removed and a superhydrophobic concrete coating (S-concrete coating) was obtained. The ordinary concrete coating (O-concrete coating) was fabricated using the same procedure but without application of water-based stone protector and nylon mesh. The fabrication processes are shown in Fig. 1.

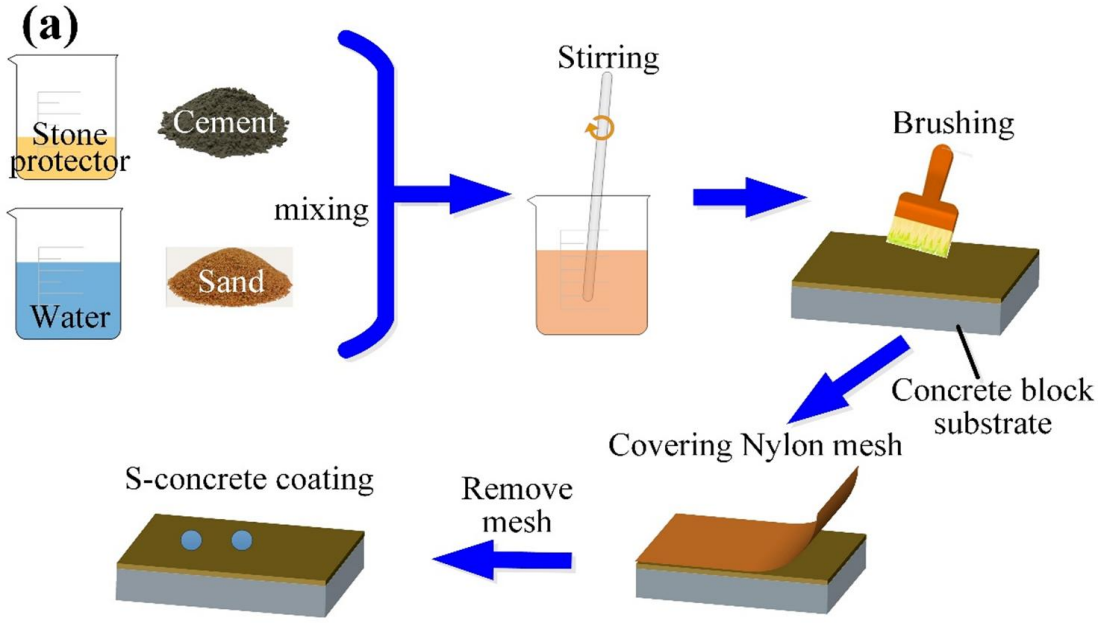

Figure 1. The schematics of the fabrication processes of the S-concrete coating.

2.2 Characterization

The contact angles and sliding angles of water droplets on the samples were measured using optical contact angle meter (Krüss, DSA100, Germany) at room temperature. The volume of water droplet was 7 μL. The surface micro-morphologies of the samples were observed using a scanning electron microscope (SEM, JSM-6360LV, Japan) at an accelerating voltage of 5 kV. The crystal structures were characterized using an X-ray diffractometer (XRD, Empyrean, Holland) with CuKα radiation (k = 0.15418 nm) at 10°-90° range and scanning step size of 2θ = 0.03939°. The elemental composition and chemical groups of the sample surfaces were examined using Fourier transform infrared spectrometer (FTIR, iN10, USA).

2.3 Surface mechanical strength test

Sandpaper abrasion and blade scratch tests were used to show the mechanical strength of the S-concrete coating. In the sandpaper abrasion test, the S-concrete coating on a circular concrete block with diameter of 60 mm was placed face-down to the 800 grit sandpaper. A 500 g weight was placed on the sample as a constant pressure. The sample was guided to move on sandpaper at a constant speed and the contact angle and sliding angle were measured every 1 m abrasion distance. In the blade scratch test, a utility blade was used to scrape the S-concrete coating with movement perpendicular to the blade edge, and the superhydrophobic effect was tested when there was noticeable powder shedding.

2.4 Anti-icing test

Two concrete blocks coated separately with the S-concrete coating and O-concrete coating were placed in an environmental chamber at an environment temperature of -10 °C. The samples had a size of 60 mm × 100 mm × 20 mm and the tilting angle was 25°. The simulated rain with a

temperature of 1 °C was applied from a 100 mL water container with 4 nozzles. The volume of rain droplet was 15 μL, and the rate of the rainfall was at 2 mL/min.

2.5 Deicing test

Two boxes without lid and bottom and with the size of 15 mm × 15 mm × 15 mm were placed separately on the S-concrete coating and O-concrete coating. Then, the concrete samples with boxes filled with water were placed horizontally in an environmental chamber at an environment temperature of -10 °C. After 4 h freezing, ice cubes with a size of 15 mm × 15 mm × 15 mm were formed and the boxes were removed. Then, the deicing force was measured using a force gauge (HP-100, Handpi Co.).

2.6 Anti-corrosion test

Two cylindrical reinforced concrete blocks with diameter of 20 mm were fabricated. Then, the S-concrete coating and O-concrete coating were separately coated on two cylindrical reinforced concrete blocks with the coating thickness of ~3 mm. All the samples were soaked in 3.5 wt% aqueous NaCl solutions at room temperature for 24 h and then tested the anti-corrosion ability. The samples were electrochemically corroded under a voltage of 26 V for 20 min in sea water (taken from the Yellow Sea, Dalian Xinghai Sea Area). After the electrochemical corrosion, the cylindrical reinforced concrete blocks were broken to observe the macro-morphology of the rebar inside. The polarization curves were obtained using a computer-controlled potentiostat (Princeton Applied Research, VersaSTAT, USA) under open circuit conditions, the sweep rate was 0.5 mV/s, and the electrochemical impedance spectroscopy (EIS) measurements were conducted in the 100 mHz to 2 MHz frequency range using a 10 mV amplitude perturbation.

3 Results and discussion

3.1 Surface morphology and wettability

Figures 2(a) and 2(b) show the macro and micro morphology of the S-concrete coating and O-concrete coating. The outside surface of the O-concrete coating was very smooth, while the outside surface of the S-concrete coating was covered with square-like convex structures with the size of 300 μm which was replicated from nylon mesh, as shown in Fig. S1. From the magnified view, both the O-concrete coating and the S-concrete coating were very rough and composed of micro/nanometer-scale particles. From the XRD patterns shown in Fig. 2(c), we learnt that the main composition of the O-concrete coating and S-concrete coating were similar, both composed of silica, calcium hydroxide, ettringite, and calcium silicate hydrate. Although the main compositions of the micro/nanometer-scale particles from the O-concrete coating and S-concrete coating are similar from XRD patterns, the C-H groups which can effectively reduce the surface energy, were only detected on the S-concrete coating. It is well known that constructing surface microstructures and lowering the surface energy at the same time is an effective way to obtain superhydrophobicity. We wondered if the O-concrete coating with micro/nanometer-scale particles can obtain superhydrophobicity after modification with water-based stone protector. Then, we modified the O-concrete coating by dipping and brushing 5 wt% aqueous solution of water-based stone protector. However, the experimental results show that the O-concrete coating after modification with water-based stone protector only shows hydrophobicity with contact angles of 90-100°, as shown in Fig. S2. Thus, the coexistence of square-like convex structures, micro/nanometer-scale particles, and low surface energy C-H groups render the S-concrete coating superhydrophobicity. Compared with the superhydrophilicity with water contact angle of ~0° on the O-concrete coating, the water droplets

on the S-concrete coating showed globular shapes with a contact angle of 160 ± 1°, and a sliding angle of 6.5 ± 0.5°. We also studied the influence of the content of water-based stone protector in the fabrication processes of the S-concrete coating on wettability. As shown in Fig. S3, the contact angles increased initially but then slightly decreased with the increase of the content, while the sliding angle decreased firstly and increased with the increase of the content. The best superhydrophobicity was obtained when the content of water-based stone protector was 5 wt% in the concrete paste. We also studied the influence of the pore size of nylon mesh in the fabrication processes of the S-concrete coating on wettability. As shown in Fig. S4, the superhydrophobicity (water contact angle ≥ 150°) was observed on the concrete-coating for the nylon mesh with pore sizes from 37 μm to 700 μm. When the pore size was too small (e.g. 20 μm) or too large (e.g. 1150 μm, and 1500 μm), only hydrophobicity was obtained.

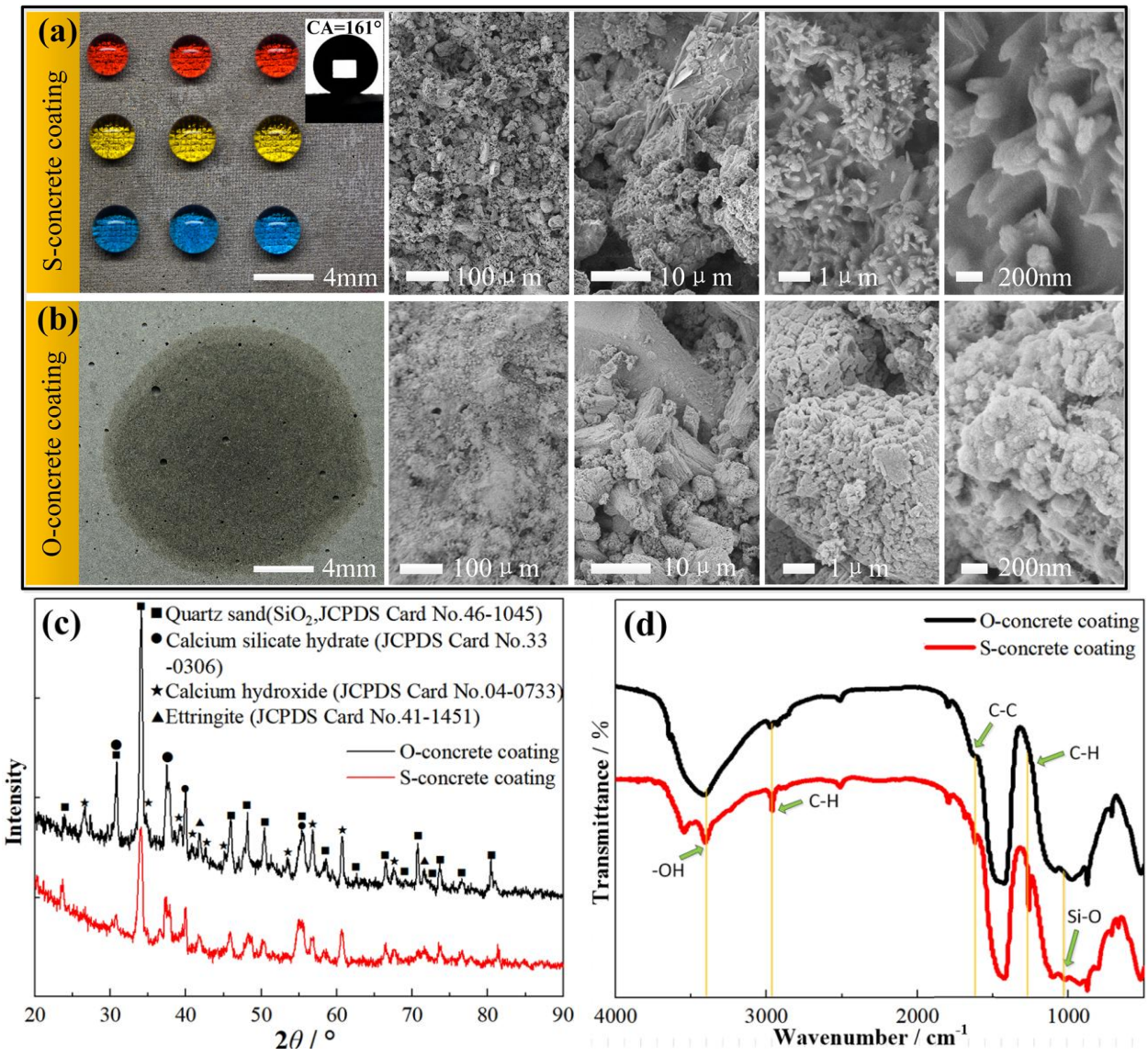

Figure 2. Surface morphology, chemical composition and wettability of the S-concrete coating and O-concrete coating: (a) the morphology and wettability of the S-concrete coating; (b) the morphology and wettability of the O-concrete coating; (c) XRD patterns of the S-concrete coating and the O-concrete coating; (d) FTIR spectra of the S-concrete coating and the O-concrete coating.

3.2 Surface mechanical strength

A scratch-resistant test was performed to demonstrate the surface mechanical strength. Blades were used to scrape the S-concrete coating with the movement perpendicular to the blade edge, followed by water dropping on the scratched area. The area that was scratched by the blade still had good superhydrophobicity, as shown in Fig. 3 (a) and **Video S1**. Fig. 3(b) and **Video S2** show the sandpaper abrasion processes of the S-concrete coating. After several meters' abrasion, water droplets on the S-concrete coating still rolled off easily without any residue. Then we carefully studied the influence of the abrasion distance on wettability. The S-concrete coating retained superhydrophobicity with a contact angle of 152° and a sliding angle of 7° even after sandpaper abrasion for 20 m. Blade scratch and sandpaper abrasion tests indicate that the developed S-concrete coating has good mechanical strength. We believe the high mechanical strength is originated from the tremendous hardness of the concrete material.

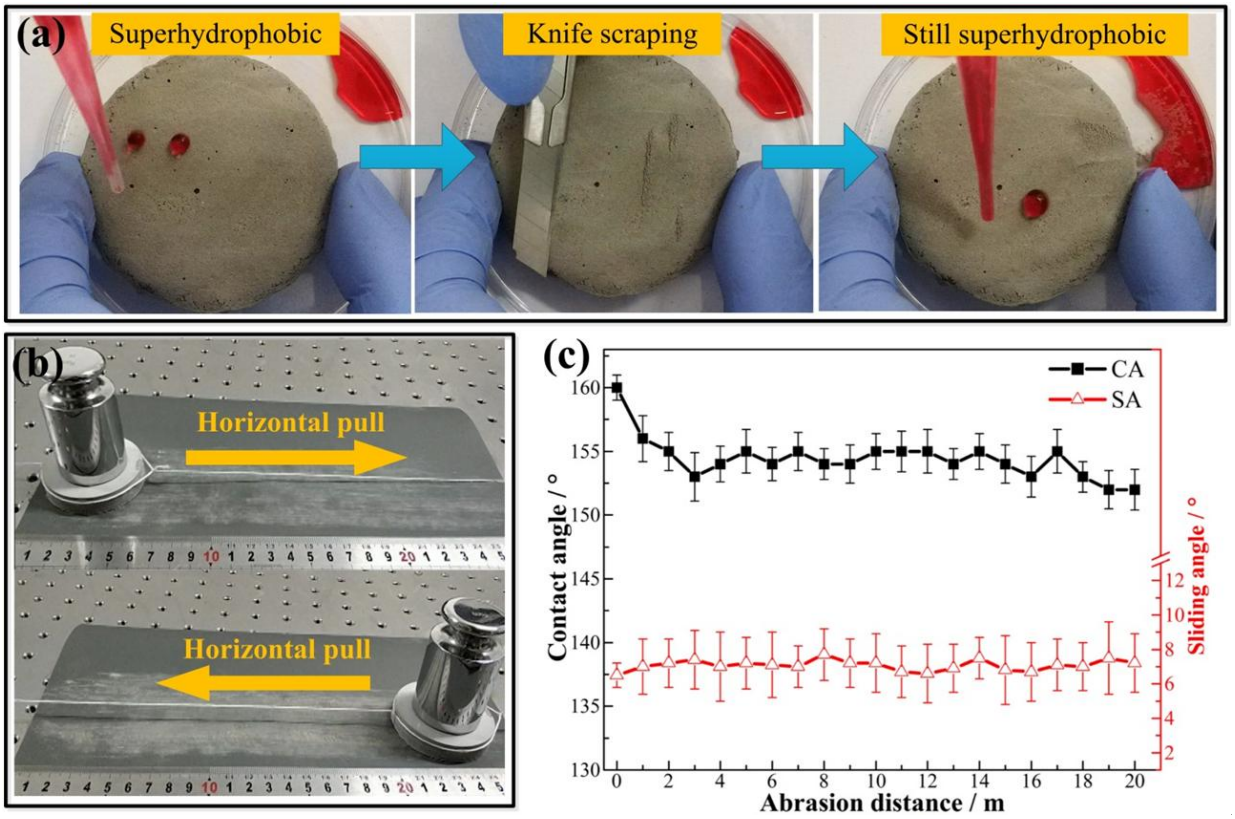

Figure 3. Surface mechanical strength tests: (a) the blade scratch processes of the S-concrete coating; (b) the sandpaper abrasion processes of the S-concrete coating; (c) the influence of abrasion distance on wettability of the S-concrete coating.

3.3 Anti-icing and deicing

Two concrete blocks coated separately with the S-concrete coating and O-concrete coating were placed in an environmental chamber with a sloping angle of 25°. Fig. 4(a) shows the schematic of the anti-icing experiment. Fig. 4(b) and **Video S3** show the anti-icing and icing processes on the S-concrete coating and O-concrete coating. The rain droplets with a temperature of 1 °C easily wetted the O-concrete coating and froze into ice under the environmental temperature of -10 °C. As the raining process continues, the ice on the O-concrete coating became thicker and thicker. However, the situation for the S-concrete coating was different. The rain droplets on the S-concrete coating rolled off completely and no ice was formed. The aforementioned results indicate the S-concrete coating has a good anti-icing ability from freezing water or cold water in a freezing environment. It's important to note that the anti-icing ability of the S-concrete coating only exists when its sloping angle larger than the sliding angle of rain droplets. When the concrete blocks were placed horizontally in the environmental chamber. Rain droplets were stayed both on the S-concrete coating and O-concrete coating and formed into ice. We then measured the deicing force in that situation and the schematic of the deicing experiment is shown in Fig. 4(c). The deicing processes on the S-concrete coating and O-concrete coating are shown in Fig. 4(d) and **Video S4**. The ice cube on the S-concrete coating was completely removed without any residue with a deicing force of 25 N, while the one on the O-concrete coating was broken with the ice residue and a deicing force of 354 N, as shown in Fig. 4(e). Low

deicing force and no ice residue on the S-concrete coating in the deicing processes would effectively reduce the deicing difficulty of horizontal roads.

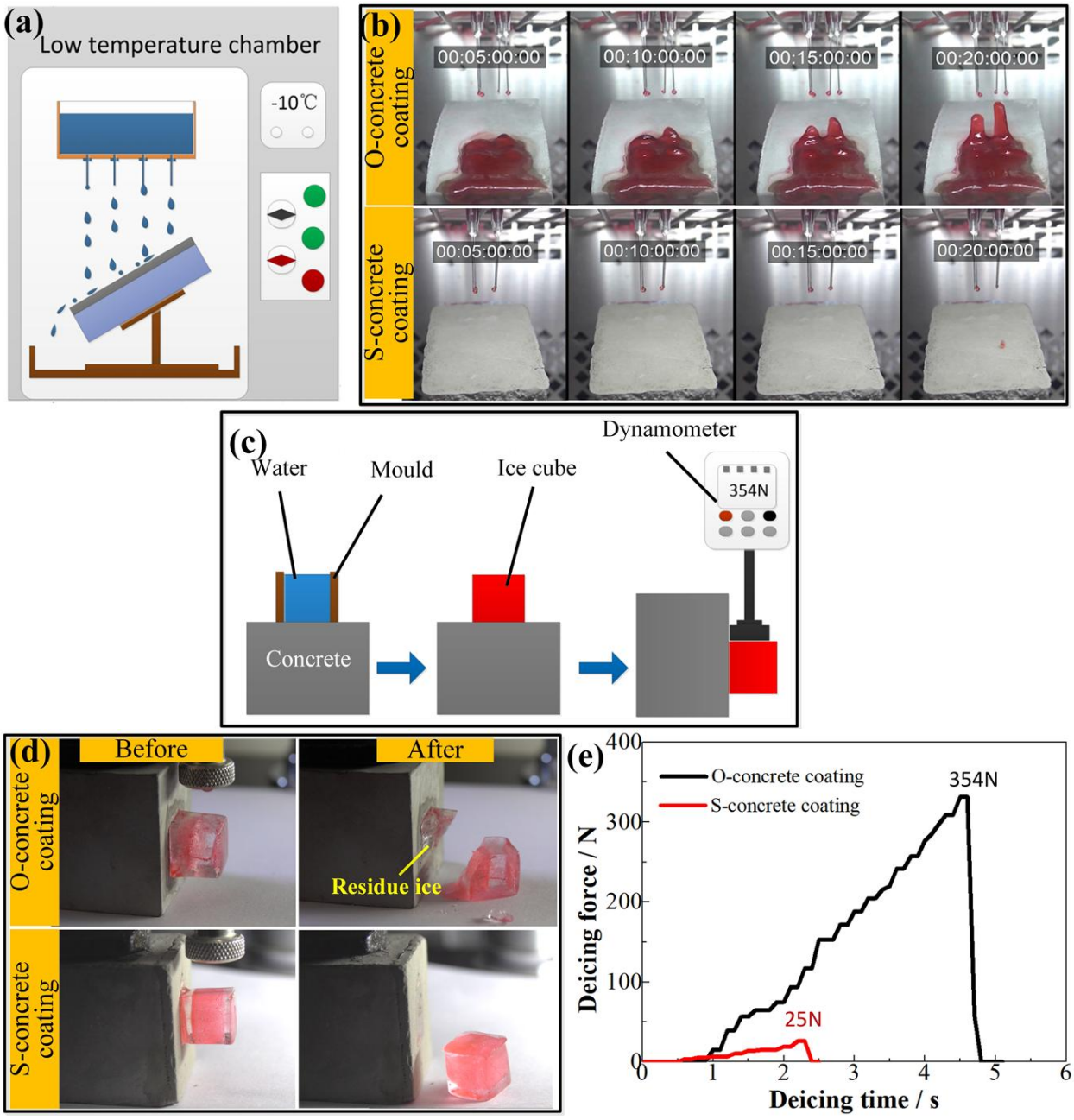

Figure 4. Anti-icing and deicing tests: (a) schematic of the anti-icing experiment; (b) the anti-icing and icing processes on the S-concrete coating and O-concrete coating; (c) schematic of the

deicing experiment; (d) the deicing processes on the S-concrete coating and O-concrete coating; (e) the deicing force for the ice cube with the ice-concrete contact area of 2.25 cm^2.

3.4 Anti-corrosion

The reinforcing rebar in the concrete plays an important role as the bone support, however, in many cases, the reinforcing rebar suffers from corrosion due to the penetration of corrosive ions into the concrete. The S-concrete coating prevents water from wetting the concrete, which in turn can block harmful components from the outside and thus protect the rebar from corrosion. Fig. 5(a) shows the schematic of the anti-corrosion test. Two reinforced concrete blocks coated separately with the S-concrete coating of 3 mm thickness and the O-concrete coating of 3 mm thickness were soaked in 3.5 wt% aqueous NaCl solutions at room temperature for 24 h first and then electrochemically corroded under a voltage of 26 V for 20 min in sea water. The electrochemical corrosion processes are shown in Fig. 5(b) and **Video S5**. We can see that with the increase of the electrochemical corrosion time, the electrolyte for the O-concrete coating became more and more turbid, indicating that the reinforcing rebar was continuously corroded. However, the electrolyte for the S-concrete coating always kept clear and translucent in the whole electrochemical corrosion processes. We then broke that two reinforced concrete blocks after electrochemical corrosion and found that the rebar inside the concrete block coated with the O-concrete coating was severely corroded and full of rust, while the rebar inside the concrete block coated with the S-concrete coating was still clean (Fig. 5(c)). Then we studied the electrochemical impedance spectra and potentiodynamic polarization curves of the rebar in the reinforced concrete blocks coated separately with the S-concrete coating and O-concrete coating in the 3.5 wt% aqueous NaCl solutions, as shown in Figs. 5(d) and 5(e). The impedance for the S-concrete coating was ten times of that for the O-concrete coating. The corrosion potential for

the S-concrete coating was 0.12 V higher than that for the O-concrete coating. The corrosion current density for the S-concrete coating was two orders magnitude lower than that for the O-concrete coating. The lower corrosion current density and higher corrosion potential and impedance are the important reasons to explain why the S-concrete coating can protect the inside rebar.

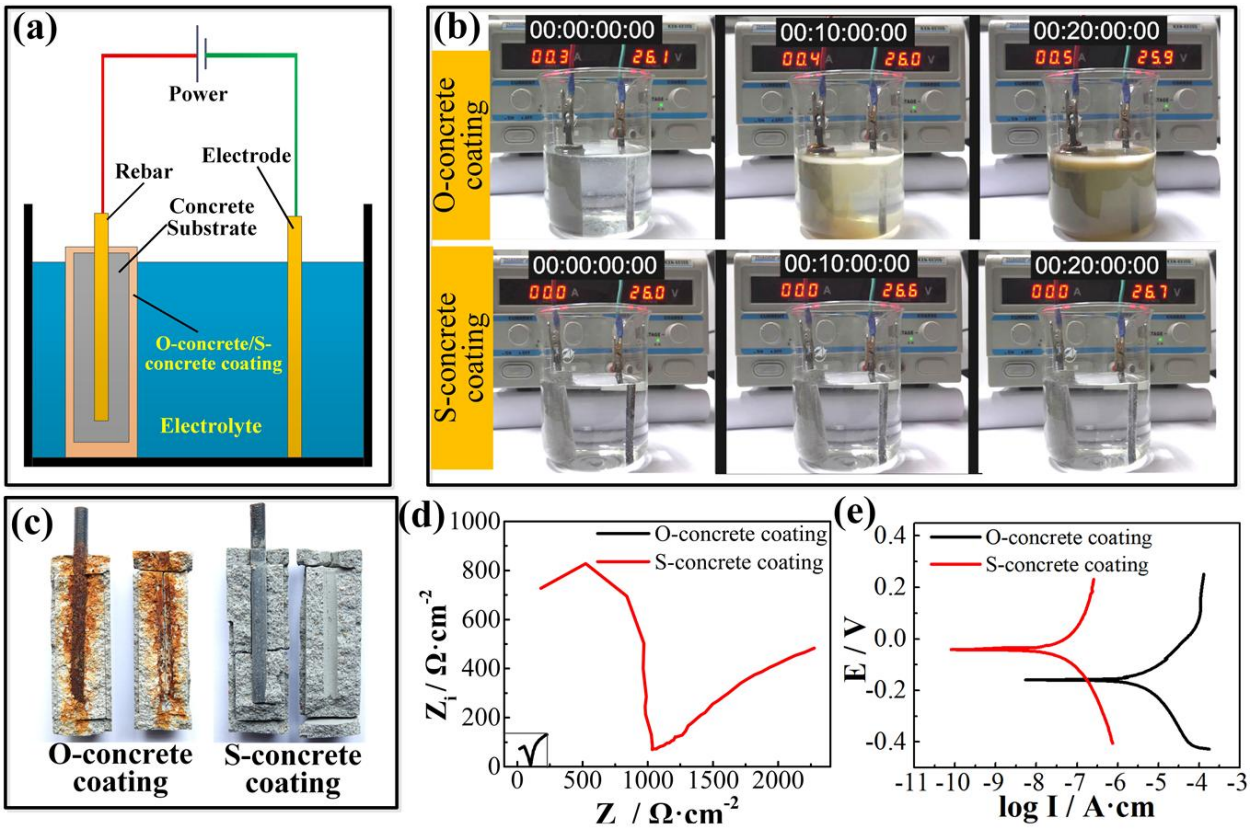

Figure 5. Anti-corrosion test: (a) schematic of the anti-corrosion test; (b) electrochemical corrosion processes under a voltage of 26 V for 20 min in sea water; (c) macro-morphology of the rebar after electrochemical corrosion; (d) the electrochemical impedance spectra of the rebar in the reinforced concrete blocks coated separately with the S-concrete coating and O-concrete coating in the 3.5 wt% aqueous NaCl solutions; (e) the potentiodynamic polarization curves of

the rebar in the reinforced concrete blocks coated separately with the S-concrete coating and O-concrete coating in the 3.5 wt% aqueous NaCl solutions.

4. Conclusions

In summary, an inexpensive and non-fluorinated superhydrophobic concrete coating (S-concrete coating) with a water contact angle of 160 ± 1° and a sliding angle of 6.5 ± 0.5° was developed using simple processes and low-cost and abundant raw materials including cement, sand, commercial water-based stone protector and nylon mesh. The superhydrophobicity was attributed to the coexistence of square-like convex structures, micro/nanometer-scale particles, and low surface energy groups. Due to the high hardness of concrete materials, the S-concrete coating with a thickness of 3 mm had a high surface mechanical strength and retained superhydrophobicity after blade scratch for several times or sandpaper abrasion for 20 m distance. The S-concrete coating also showed a good anti-icing ability for concrete substrate with the sloping angle larger than the sliding angle from freezing water or cold water in a freezing environment, and also showed a low de-icing force for horizontal concrete substrate. The water-repellent property of the S-concrete coating further made it possible to protect the rebar in the reinforcing concrete from corrosion. The S-concrete coating can be easily applied on the outside surface of architecture, which not only protects the reinforced concrete but also would not affect the strength and carrying capacity of architecture. Therefore, this economic and environmental-friendly coating is expected to be applied on buildings, bridges and many other concrete-based projects in large scale for anti-icing and anti-corrosion purposes.

Acknowledgements

This project is financially supported by National Natural Science Foundation of China (NSFC, 51605078, 21774051), the Science Fund for Creative Research Groups of NSFC (51621064),

Young Elite Scientists Sponsorship Program by CAST (YESS, 2017QNRC001), Aviation Science Fund (2017ZE63012). Y.L. acknowledges the support from EPSRC project EP/N024915/1.

References

(1) Andersson, A.; Chapman, L. The use of a temporal analogue to predict future traffic accidents and winter road conditions in Sweden. Meteorological Appl. 18 (2011) 125-136. doi：10.1002/met.186

(2) Zhang, P.; Cong, Y.; Vogel, M.; Liu, Z.; Müller, H. S.; Zhu, Y.; Zhao, T. Steel reinforcement corrosion in concrete under combined actions: The role of freeze-thaw cycles, chloride ingress, and surface impregnation. Constr. Build. Mater. 148 (2017) 113-121. doi：10.1016/j.conbuildmat.2017.05.078

(3) Lu, Y.; Sathasivam, S.; Song, J.; Crick, C.; Claire J.; Ivan, P. Robust self-cleaning surfaces that function when exposed to either air or oil. Science 347 (2015) 1132-1135. doi：10.1126/science.aaa0946

(4) Deng, X.; Mammen, L.; Butt, H.; Vollmer, D. Candle soot as a template for a transparent robust superamphiphobic coating. Science 335 (2012) 67-70. doi:10.1126/science.1207115

(5) Pan, S.; Guo, R.; Björnmalm, M.; Richardson, J. J.; Li, L.; Peng, C.; Bertleff-Zieschang, N.; Xu, W.; Jiang, J.; Caruso, F. Coatings super-repellent to ultralow surface tension liquids. Nature Mater. 17 (2018) 1040-1047. doi:10.1038/s41563-018-0178-2

(6) Peng, C.; Chen, Z.; Tiwari, M. K. All-organic superhydrophobic coatings with mechanochemical robustness and liquid impalement resistance. Nature Mater. 17 (2018) 355-360. doi:10.1038/s41563-018-0044-2

(7) Coclite, A. M.; Shi, Y.; Gleason, K. K. Grafted crystalline poly-perfluoroacrylate structures for superhydrophobic and oleophobic functional coatings. Adv. Mater. 24 (2012) 4534-4539. doi:10.1002/adma.201200682

(8) Chen, S.; Li, X.; Li, Y.; Sun, J. Intumescent flame-retardant and self-healing superhydrophobic coatings on cotton fabric. ACS Nano 9 (2015) 4070-4076. doi:10.1021/acsnano.5b00121

(9) Seo, K.; Kim, M.; Kim, D. H. Candle-based process for creating a stable superhydrophobic surface. Carbon 68 (2014) 583-596. doi:10.1016/j.carbon.2013.11.038

(10) Iqbal, R.; Majhy, B.; Sen, A. K. Facile fabrication and characterization of a PDMS-derived candle soot coated stable biocompatible superhydrophobic and superhemophobic surface. ACS Appl. Mater. Inter. 9 (2017) 31170–31180. doi:10.1021/acsami.7b09708

(11) Li, J.; Zhao, Z.; Li, D.; Tian, H.; Zha, F.; Feng, H.; Guo, L. Smart candle soot coated membranes for on-demand immiscible oil/water mixture and emulsion switchable separation. Nanoscale 9 (2017) 13610. doi:10.1039/C7NR04448H

(12) Hu, X.; Tang, C.; He, Z.; Shao, H.; Xu, K.; Mei, J.; Lau, W. M. Highly stretchable superhydrophobic composite coating based on self-adaptive deformation of hierarchical structures. Small 13 (2017) 1602353. doi:10.1002/smll.201602353

(13) Wei, W.; Lockwood, K.; Boyd, L. M.; Davidson, M. D.; Movafaghi, S.; Vahabi, H.; Khetani, S. R.; Kota, A. K. Superhydrophobic coatings with edible materials. ACS Appl. Mater. Inter. 8 (2016) 18664-18668. doi:10.1021/acsami.6b06958

(14) Chen, B.; Qiu, J.; Sakai, E.; Kanazawa, N.; Liang, R.; Feng, H. Robust and superhydrophobic surface modification by a "paint + adhesive" method: applications in self-cleaning after oil contamination and oil–water separation. ACS Appl. Mater. Inter. 8 (2016) 17659-17667. doi:10.1021/acsami.6b04108

(15) Nine, M. J.; Cole, M. A.; Johnson, L.; Tran, D. N. H.; Losic, D. Robust superhydrophobic graphene-based composite coatings with self-cleaning and corrosion barrier properties. ACS Appl. Mater. Inter. 7 (2015) 28482-28493. doi:10.1021/acsami.5b09611

(16) Ghosh, A.; Ganguly, R.; Schutzius, T. M.; Megaridis, C. M. Wettability patterning for high-rate, pumpless fluid transport on open, non-planar microfluidic platforms. Lab on A Chip 14 (2014) 1538-1550. doi:10.1039/c3lc51406d

(17) De, F. R.; Hoyos, M.; García, N.; Tiemblo, P. Superhydrophobic and highly luminescent Polyfluorene/Silica hybrid coatings deposited onto glass and cellulose-based substrates. Langmuir 31 (2015) 3718-26. doi:10.1021/acs.langmuir.5b00293

(18) Zhi, D.; Lu, Y.; Sathasivam, S.; Parkin, I. P.; Zhang, X. Large-scale fabrication of translucent and repairable superhydrophobic spray coatings with remarkable mechanical, chemical durability and UV resistance. J. Mater. Chem. A 5 (2017) 10622-10631. doi:10.1039/C7TA02488F

(19) Yang, H.; Liang, F.; Chen, Y.; Wang, Q.; Qu, X.; Yang, Z. Lotus leaf inspired robust superhydrophobic coating from strawberry-like Janus particles. NPG Asia Mater. 7 (2015) e176. doi:10.1038/am.2015.33

(20) Xu, L.; Zhu, D.; Lu, X.; Lu, Q. Transparent, thermally and mechanically stable superhydrophobic coating prepared by an electrochemical template strategy. J. Mater.Chem. A 3 (2015) 3801-3807. doi:10.1039/C4TA06944G

(21) Tuvshindorj, U.; Yildirim, A.; Ozturk, F. E.; Bayindir, M. Robust Cassie state of wetting in transparent superhydrophobic coatings. ACS Appl. Mater. Inter. 6 (2014) 9680-9688. doi:10.1021/am502117a

(22) Liu, H.; Huang, J.; Chen, Z.; Chen, G.; Zhang, K.; Al-Deyab, S. S.; Lai, Y. Robust translucent superhydrophobic PDMS/PMMA film by facile one-step spray for self-cleaning and efficient emulsion separation. Chem.Eng. J. 330 (2017) 26-35. doi:10.1016/j.cej.2017.07.114

(23) Liu, F.; Sun, F.; Pan, Q. Highly compressible and stretchable superhydrophobic coating inspired by bio-adhesion of marine mussels. J. Mater. Chem. A 2 (2014) 11365-11371. doi:10.1039/c4ta01552e

(24) Song, J.; Zhao, D.; Han, Z.; Xu, W.; Lu, Y.; Liu, X.; Liu, B.; Carmalt, C. J.; Deng, X.; Parkin, I. P. Super-robust superhydrophobic concrete. J. Mater. Chem. A 5 (2017) 14542-14550. doi:10.1039/C7TA03526H